Diffraction model of elastic hadron-hadron scattering

M. Kawasaki
Physics Department, Gifu University, Yanagido, Gifu 501-11, Japan

T. Maehara
Faculty of School Education, Hiroshima University, Hiroshima 734, Japan

M. Yonezawa
Department of Physics, Hiroshima University, Higashi-Hiroshima 724, Japan
(Received 16 August 1993)

A simple diffractive amplitude for high-energy elastic hadron-hadron scattering is given, which includes some typical cases of diffraction. We show the similarities of the model to a realistic geometrical model which explains pp and $\bar{p}p$ scattering in the energy region $\sqrt{s} \leq 1.8$ TeV well and could provide a reasonable extrapolation to higher energies.

PACS number(s): 13.85.Dz, 12.40.Nn

I. INTRODUCTION

The black disk may be the asymptotic shape of elastic hadron-hadron interactions [1]. At least some models predict it under a rising total cross section and elasticity with energy [1,2]. If the black disk is realized asymptotically for hadron-hadron interactions, it will be an interesting question how the asymptopia will be approached [3].

Since the uniform disk has the profile of the most compact state with the minimum radius allowed by unitarity, unitarity-saturating features of strong interactions may be observed even before the onset of asymptopia [4]. In this work we give a simple parametric representation for the elastic hadron-hadron diffraction scattering amplitude which ends at the uniform disk and shows its qualitative similarities with a realistic geometrical model at the CERN Large Hadron Collider ($\sqrt{s} = 15.4$ TeV), the Superconducting Super Collider (40 TeV), and higher energy regions.

II. THE BESSEL FUNCTION MODEL

We neglect the effects of the spin of the hadron and of the real part of the scattering amplitude. The diffraction model for elastic hadron-hadron scattering, which is discussed here and is called the Bessel function model hereafter, is given by the impact-parameter scattering amplitude $a(b)$ as

$$-2ia(b) = 1 - s(b) = \begin{cases} \frac{\sigma_t}{4\pi}\frac{2\nu}{R^2}\left(1-\frac{b^2}{R^2}\right)^{\nu-1} & \text{for } b < R\ , \\ 0 & \text{for } b > R\ , \end{cases} \tag{1}$$

where $s(b)$ is the impact-parameter S matrix, σ_t the total cross section, R the interaction radius, and ν a real parameter in the range $\nu \geq 1$ characterizing the shape of the interaction.

The differential cross section is related to the impact-parameter amplitude $a(b)$ by

$$\frac{d\sigma}{dt} = 4\pi\left|\int_0^\infty bdba(b)J_0(\sqrt{-t}b)\right|^2 , \tag{2}$$

and is given by

$$\frac{d\sigma}{dt} = \frac{\sigma_t^2}{16\pi}\{\Gamma(\nu+1)(2/z)^\nu J_\nu(z)\}^2\ , \quad z \equiv R\sqrt{-t}\ , \tag{3}$$

where t is the squared momentum transfer, J_ν the Bessel function of the order ν, and Γ the gamma function.

If we define the forward slope B and the forward curvature C by expressing the differential cross section at small momentum transfers as [1]

$$\frac{d\sigma}{dt} = \left(\frac{d\sigma}{dt}\right)_{t=0} e^{(Bt+Ct^2+\cdots)}\ , \tag{4}$$

we obtain, from (3),

$$B = \frac{R^2}{2(\nu+1)}\ , \quad C = -\frac{R^4}{16}\frac{1}{(\nu+1)^2(\nu+2)}\ . \tag{5}$$

Also we have the following expression for the elastic cross section:

$$\sigma_{\rm el} = \int_{-\infty}^0 \left(\frac{d\sigma}{dt}\right)dt = \frac{\sigma_t^2}{4\pi R^2}\frac{\nu^2}{2\nu-1}\ . \tag{6}$$

This gives the cutoff interaction radius R in terms of σ_t and the elasticity $x \equiv \sigma_{\rm el}/\sigma_t$ as

$$R = \left(\frac{\sigma_t}{4\pi x}\frac{\nu^2}{2\nu-1}\right)^{1/2}\ . \tag{7}$$

The radius measured in units of $\sqrt{\sigma_t}/x$ is a monotonically increasing function of ν for $\nu \geq 1$. The slope and curvature are also given by

$$B = \frac{\sigma_t}{4\pi x} \frac{\nu^2}{2(\nu+1)(2\nu-1)} , \tag{8}$$

$$C = -\frac{1}{16}\left(\frac{\sigma_t}{4\pi x}\right)^2 \left(\frac{\nu^2}{2\nu-1}\right)^2 \frac{1}{(\nu+1)^2(\nu+2)} .$$

The amplitude (1) involves three important cases of high-energy diffraction scattering [1]. (i) The case $\nu = 1$ corresponds to the uniform-disk (UD) model. The uniform disk is the minimum-radius solution for given σ_t and x allowed by unitarity [3]; (ii) when ν takes 2, the impact-parameter amplitude is parabolic in b and saturates the MacDowell-Martin (MM) bound [5], $B_{\rm MM} \equiv (\sigma_t/18\pi x)$, which is the lower limit for the forward logarithmic slope B for given σ_t and x; (iii) if we take the limit $\nu \to \infty$, the impact-parameter amplitude becomes Gaussian, giving an exponentially falling differential cross section in $|t|$. The last case can be easily seen if we rewrite the impact-parameter amplitude in terms of x and σ_t as

$$-2ia(b) = \begin{cases} \frac{2x(2\nu-1)}{\nu}\left(1 - \frac{4\pi x}{\sigma_t}\frac{2\nu-1}{\nu^2}b^2\right)^{\nu-1} & \text{for } b < R , \\ 0 & \text{for } b > R . \end{cases} \tag{9}$$

In the limit of $\nu \to \infty$ we have

$$-2ia(b) = 4xe^{-(8\pi x/\sigma_t)b^2} , \quad \frac{d\sigma}{dt} = \frac{\sigma_t^2}{16\pi} e^{(\sigma_t/16\pi x)t} . \tag{10}$$

The unitarity condition $0 \leq -2ia(b) \leq 1$ imposed for the geometrical absorber picture $[0 \leq s(b) \leq 1]$ gives the restriction on the elasticity as

$$0 \leq x \leq \frac{\nu}{4\nu - 2} . \tag{11}$$

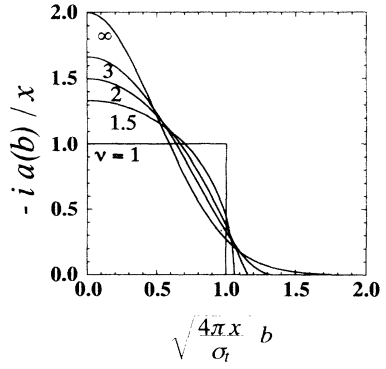

FIG. 1. The impact-parameter amplitudes (1) divided by $2x$, $-ia(b)/x$, of the Bessel function model are shown for $\nu = 1, 1.5, 2, 3$, and ∞.

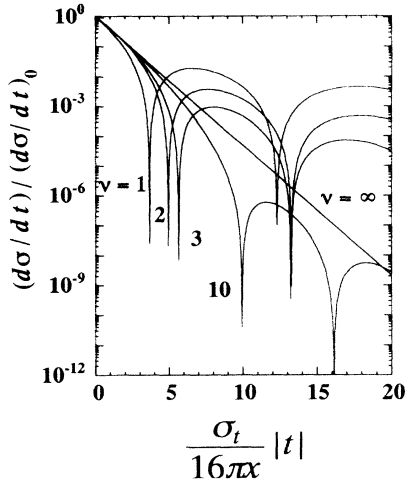

FIG. 2. The differential cross sections of the Bessel function model (3) for $\nu = 1, 2, 3, 10$, and ∞.

These three cases, (i), (ii), and (iii), often play the role of the reference frames when we discuss high-energy diffraction scattering. The reason why we are particularly interested in model (1), compared with other parametrizations such as $a(b) \propto [1 - (b/R)]^n$ or $1 - (b/R)^n$, is that it involves these cases of the diffraction amplitude and affords their natural generalization. Further it represents some features of the behavior of the differential cross sections at very high energies with ν monotonically decreasing with increasing x as will be discussed in the following.

The impact-parameter amplitude (1) is shown in Fig. 1, the differential cross section (3) in Fig. 2, and the trajectory $(B/B_{\rm MM} - R/B_{\rm MM}^{1/2})$ given by Eqs. (7) and (8) in Fig. 3. The slope B takes the minimum value $B_{\rm MM}$ at $\nu = 2$ and has the same value $(9/8)B_{\rm MM}$ for $\nu = 1$ and ∞ for given σ_t/x.

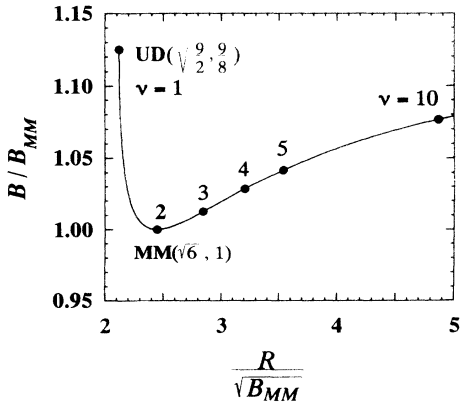

FIG. 3. The slope-radius relation of the Bessel function model. Here UD denotes the uniform-disk limit and MM the MacDowell-Martin bound.

III. COMPARISON WITH REALISTIC GEOMETRICAL MODEL

Let us consider what will be expected for the differential cross section of hadron-hadron scattering at very high energies. Unfortunately, we have no experimental data at energies higher than $\sqrt{s} = 1.8$ TeV. Therefore, we use the predictions of the generalized geometrical scaling (GGS) model [6,7], which has the basic features of geometrical pictures including the Chou-Yang model [8]. In this model the impact-parameter amplitude is given by

$$-2ia(b) = 1 - e^{-\Omega(s,b)}$$

with

$$\Omega(s,b) = w(s)g(b/r(s)) \ , \tag{12}$$

where the strength $w(s)$ and the scaling length parameter $r(s)$ are taken to reproduce the elasticity and the total cross section for a given eikonal shape function $g(b)$.

If we take

$$g(b) = \frac{1}{8}(\mu b)^3 K_3(\mu b) \ , \tag{13}$$

where K_3 is the modified Bessel function of the order 3, and assume $r(s) = 1$, with μ being the mass of the dipole electromagnetic form factor of the proton, we have the Chou-Yang model. This model does not explain, however, the $\bar{p}p$ experiments at the CERN S$\bar{p}p$S and the Fermilab Tevatron Collider [6].

If we assume μ as energy dependent or, equivalently, introduce the scaling length parameter $r(s)$, then the amplitude (12) reasonably reproduces the differential cross sections at small momentum transfers $|t| \leq 1.5$ (GeV/c)^2 in the energy region from the CERN Intersecting Storage Ring (ISR) to the Tevatron ($\sqrt{s} = 20 - 2000$ GeV) [6]. This generalization of the Chou-Yang model will be called the Chou-Yang (CY) generalized geometrical scaling (GGS) model.

The quantity which specifies the structure of the scattering amplitude under the GGS hypothesis is the elasticity x, and for a fixed x the differential cross section shows the geometrical scaling behavior [9]; i.e., it is the functon of $\sigma_t t$. If x increases, it implies the increase of the strength $w(s)$. This means the flattening of the impact-parameter amplitude rises at a small impact parameter and extends to a larger one, finally giving the black-disk structure at $x \sim 0.5$. Therefore, the results of the following analysis, though obtained for a specific model, will hold approximately for any physically sensible models having $\Omega(s,b)$ divergent as s tends to infinity. In this respect we note that there appears a kind of eikonal-shape independence of geometrical scattering amplitude from $x \sim 0.35$ at small momentum transfers including the dip-bump region. This is caused by the exponentiation effect just stated. We show the situation in Fig. 4 where we give the differential cross sections for the eikonal function,

$$g(b/r(s)) = \frac{2}{(n-1)!}\left\{\frac{\mu b/r(s)}{2}\right\}^n K_n(\mu b/r(s)) \ , \tag{14}$$

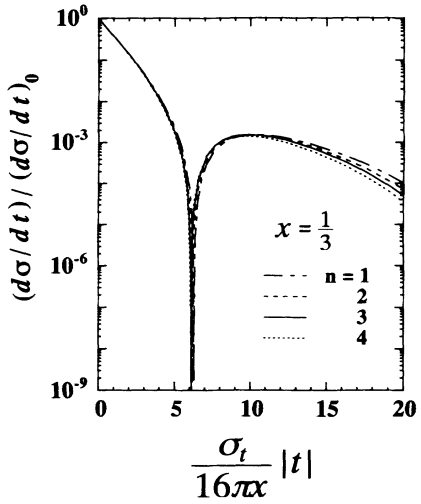

FIG. 4. Eikonal-shape-independent feature of the geometrical model. The results are given for $g(b,s)$ of Eq. (14) for $n = 1$, 2, 3, and 4 at $x = 1/3$.

with $n = 1 - 4$ at $x = 1/3$, which is taken to be somewhat smaller than 0.35. The cases $n = 1$ and 2 have special interest in connection with the Chou-Yang model of meson-meson and meson-nucleon scattering, respectively, if the meson electromagnetic form factor is approximated by a pole. We emphasize that neither $n = 2$ nor 4 can explain the pp and $\bar{p}p$ data at the ISR region even at small momentum transfers; therefore, the eikonal-shape independence of the differential cross section indicated in Fig. 4 is not trivial [10]. This flattening of the interaction profile caused by the growing eikonal in the exponent in Eq. (12) reflects a unitarity-saturating property of the strong interaction.

Now we give some features of the GGS differential cross section [3,6,7].

(a) As x increases, $B/B_{\rm MM}$ of the CY GGS model decreases to the minimum value ~ 1.03 around $x = 0.38$, then turns to increase to the asymptotic value (9/8) of the uniform disk at $x = 0.5$.

(b) The dip structure has already been clearly observed at ISR experiments, and will persist at all higher energies, if the GGS hypothesis has validity. If the elasticity x increases as energy increases, the value $\sigma_t|t_{\rm dip}|/x$ of the dip position steadily decreases and finally arrives at that of the black disk.

(c) The height of the second maximum of the normalized differential cross section $(d\sigma/dt)/(d\sigma/dt)_{t=0}$ increases as the elasticity increases. This is often emphasized as one of the important consequences of the geometrical picture.

(d) The curvature C changes its sign from positive to negative as x increases. This occurs around $x = 0.3$ for the case of the CY GGS model.

These properties (a)–(d) are also shared by the Bessel function model (1), if the elasticity x is related in such a way that x increases as ν decreases [the maximum elasticity given by Eq. (11) has such a feature]. In the following we give the properties of the Bessel function model

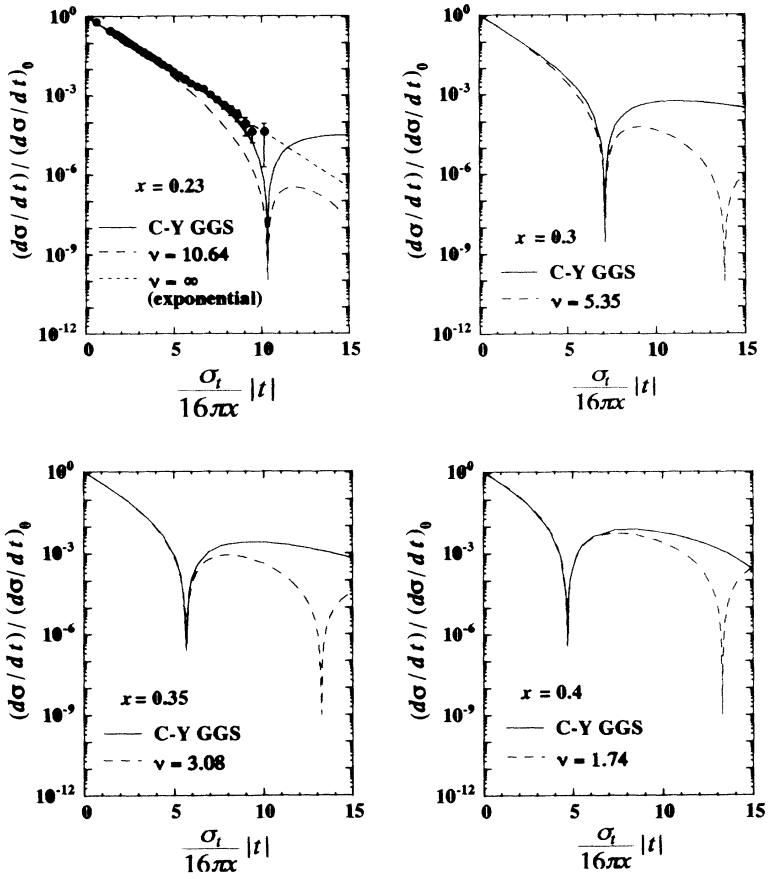

FIG. 5. Comparison of the Bessel function model with the Chou-Yang GGS model for $\bar{p}p$ scattering. Here the parameter ν of the Bessel function model is chosen to give the same first dip position as the GGS model. The experimental data given for $x = 0.23$ are those of $\bar{p}p$ at 1.8 TeV taken from Ref. [12].

corresponding to (a)–(d).

(α) The behavior (a) of the forward slope looks like the change of B in (8) as ν decreases from infinity to 1: the ratio $B/B_{\rm MM}$ starts from (9/8) at $\nu = \infty$, reaches the minimum value 1 at $\nu = 2$, then increases to (9/8) of the uniform disk as ν tends to 1.

(β) The first dip of the cross section (3) is monotonically moving forward as ν decreases from infinity (where dips are pushed away to infinite $|t|$) to 1.

(γ) The second diffraction maximum of the Bessel function model increases as ν decreases.

(δ) The curvature C is always negative as given in Eq. (8).

Hence common features exist between the Bessel function model (1) and the GGS picture. There are, of course, differences if we compare quantitatively. The ratio $B/B_{\rm MM}$ takes the value only between 9/8 and 1 in the diffraction picture (1), while the CY GGS model takes the value higher than 1.03 and even higher than 9/8 below ~ 10 TeV. When ν is very large, $B/B_{\rm MM}$ is near 9/8 and Eq. (3) gives a dip at very large $|t|$ while the CY GGS model gives the ratio $B/B_{\rm MM} \sim 9/8$ at $x = 0.25$ (10 TeV) and the model predicts a dip at $|t| \sim 0.5$ (GeV/c)^2 at this energy. Here the value in parentheses is the c.m. system (c.m.s.) energy of $\bar{p}p$ scattering giving the same elasticity, when we dare to extrapolate the empirical fit formula

TABLE I. Comparison of the Bessel function model with Chou-Yang GGS model where the only free parameter ν of the Bessel function model is chosen to give the same dip position as that of the GGS model. The cases shown correspond to those in Fig. 5. Here $x_{\rm max}$ is the allowed maximum elasticity which satisfies the unitarity, Eq. (11). If the elasticity is larger than $x_{\rm max}$, the Bessel function model violates the geometrical model unitarity restriction $-2ia(b) < 1$ for some range of b at its small values.

Chou-Yang GGS model					
x	0.23	0.3	0.35	0.4	0.5
$\sigma_t\|t_{\rm dip}\|/16\pi x$	10.3	7.2	5.6	4.7	3.7
$B/B_{\rm MM}$	1.16	1.11	1.06	1.03	1.125
Bessel function model					
ν	10.64 (∞)	5.35	3.08	1.74	1
$x_{\rm max}$	0.262 (0.25)	0.276	0.298	0.351	0.5
$B/B_{\rm MM}$	1.08 (1.125)	1.045	1.014	1.002	1.125

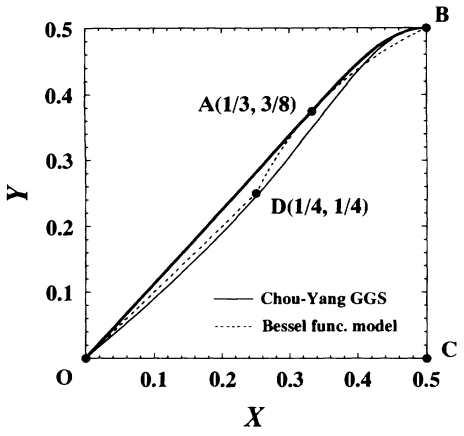

FIG. 6. The X-Y diagram of the Bessel function model (the dotted curves) and the Chou-Yang GGS model prediction (the thin solid curve). The CY GGS and the Chou-Yang model give the same curve. The thick straight line O-A is the MacDowell-Martin bound [5] and the thick solid curve A-B is the Chao-Yang bound [14].

for the cross sections obtained below 1.8 TeV [11]. We have also used the value of the total cross section of the empirical formula in the calculation at 10 TeV. The forward curvature C of the Bessel function model is negative definite and monotonically increasing as ν increases from 1 to ∞, where the curvature vanishes, but the CY GGS model gives zero curvature only around $x = 0.3$ (50 TeV).

Therefore, the similarity is gross and global and the local quantitative agreement is not much expected, but a direct comparison of the Bessel function model with the GGS model is still worthwhile to give a better understanding of their mutual relation. We show the differential cross sections of the Bessel function model and the predictions of the CY GGS model in Fig. 5 for $x = 0.23$ ($\sqrt{s} = 1.8$ TeV), 0.3 (50), 0.35 (2×10^3), and 0.4 (4×10^6) with those of Eq. (3) having the *same dip positions* as those of CY GGS. Clearly the agreement is improved as x increases, though quantitatively the agreement is not so good as seen in the forward slope shown in Table I, where we give some results of the GGS calculation and of the Bessel function model corresponding to Fig. 5. If we restrict the region of momentum transfer to $0 \le \sigma_t|t|/16\pi x \le 8$, we can see a reasonable agreement. This restriction of the region suggests to us to regard the low-energy region below 1 TeV as $\nu \sim \infty$, nearly degenerate as suggested by an approximate scaling with $\sigma_t t/x$ [13], by ignoring the dip structure appearing at $\sigma_t|t|/16\pi x > 8$.

As another way of looking at the resemblance between two models, we give the X-Y plot of Chao and Yang [14] in Fig. 6 where $X = x$ and $Y = \sigma_t/16\pi B$. This figure involves essentially the contents of (a) and (α) stated above. At low elasticities below ~ 0.25, the CY GGS curve (which gives the same as the Chou-Yang model [8] in this case) roughly moves along the dotted O-D line which corresponds to $\nu = \infty$ of the Bessel function model. (Actually the envelope of the line OP forms the allowed area for the Bessel function model when P moves on the Bessel function curve.) As x increases, the CY GGS curve shifts upwards, but not as fast as the Bessel function model bends. It crosses over the Bessel function line around $x \sim 0.4$ and approaches the Chao-Yang bound given by the thick solid A-B curve which, for $x > 1/3$, takes up the MacDowell-Martin bound given by the O-A line. The black disk locates at B. The area enclosed by O-A-B-C-O is allowed by unitarity [14].

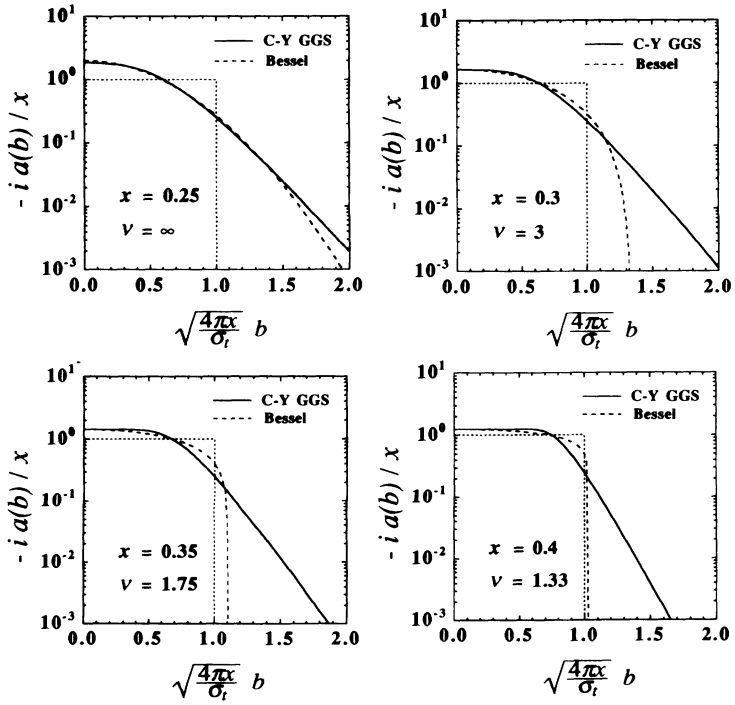

FIG. 7. Comparison of the interaction profiles of the Chou-Yang GGS model for the elasticity x with the Bessel function model with ν related to x by $\nu = 2x/(4x-1)$ for ($x = 0.25$, $\nu = \infty$), (0.3,3), (0.35,1.75), and (0.4,1.33). The solid curves correspond to the CY GGS model and the dotted curves the Bessel function model.

As the last comparison of two models, we show their interaction profiles in Fig. 7. Since their similarities are global, there is no unique way for making a comparison. In Fig. 5 we have compared the two models giving the same dip positions. Here we give the CY GGS amplitude with the elasticity x and the Bessel function amplitude with ν related to x by $\nu = 2x/(4x-1)$, since the Bessel function with such a value of ν may be considered as the closest to the CY model from a unitarity viewpoint. Comparison of two profiles indicates that their resemblance is gross and does not increase as x increases in the range given in Fig. 7. They approach the uniform disk in different ways as also suggested by the X-Y diagram in Fig. 6.

If the asymptopia is signaled by (1) the sharp-edge structure of the interaction which may be accompanied by negative curvature [2] and (2) the eikonal-shape independence (hence process independence) feature of the interaction, the GGS calculation for pp and $\bar{p}p$ scattering suggests $x \sim 0.3$ for the former and 0.35 for the latter.

IV. SUMMARY

We have shown that the Bessel function model (1) has many interesting features as a simple diffraction model. Although the physical meaning of this model, beyond special cases (i)–(iii), needs to be studied further, the model serves at least as an illustration for realistic geometrical models. It is to be stressed, though not directly related with the Bessel function model itself, that the features of the differential cross section will become nearly independent of the shape of the eikonal from $x \sim 0.35$ as envisaged from Figs. 4 and 5: at higher elasticities all elastic baryon-baryon and meson-baryon interactions will assume common structures which may resemble more and more the Bessel function model. If such geometrization of the scattering amplitude starts, the elastic differential cross section may not provide useful information on the hadron interaction. In other words, the study in the energy region below that reached at the Superconducting Super Collider is quite important.

[1] M. M. Block and R. N. Cahn, Rev. Mod. Phys. **57**, 563 (1985).

[2] M. M. Block, F. Halzen, and B. Margolis, Phys. Lett. B **252**, 481 (1990).

[3] M. Kawasaki, T. Maehara, and M. Yonezawa, Phys. Rev. D **48**, 4082 (1993).

[4] Another unitarity-saturating feature of strong interaction is the Froissart-bound-like behavior of the total cross section rising as $\ln^2(s/s_0)$, M. Froissart, Phys. Rev. **123**, 1053 (1961), though its coefficient is far less than the value $(1/m_\pi)^2$ suggested by naive consideration. For an interpretation of small coefficients, see Ref. [2].

[5] S. W. MacDowell and A. Martin, Phys. Rev. **135**, B960 (1964).

[6] M. Kawasaki, T. Maehara, and M. Yonezawa, Phys. Rev. D **47**, R3 (1993). See also V. Barger, J. Luthe, and R. J. N. Phillips, Nucl. Phys. **B88**, 237 (1975); T. T. Chou and C. N. Yang, Phys. Lett. B **244**, 113 (1990).

[7] M. Kawasaki, T. Maehara, and M. Yonezawa, Phys. Rev. D **48**, 3098 (1993).

[8] T. T. Chou and C. N. Yang, Phys. Rev. **170**, 1591 (1968); L. Durand III and R. Lipes, Phys. Rev. Lett. **20**, 637 (1968); F. Hayot and U. P. Sukhatme, Phys. Rev. D **10**, 2183 (1974).

[9] G. Auberson, T. Kinoshita, and A. Martin, Phys. Rev. D **3**, 3185 (1971); J. Dias de Deus, Nucl. Phys. **B59**, 231 (1973); A. J. Buras and J. Dias de Deus, *ibid.* **B71**, 481 (1974).

[10] The c.m.s. total energy $\sqrt{s}$ varies by a factor 10^2 from ISR to Tevatron, during which we find no apparent indication for the change of the shape of the eikonal Ω specified by $g(b)$. When the energy goes up further by a factor 10^2 over 100 TeV, there is no evidence at present suggesting new interaction mechanisms which may cause significant change in the shape of the eikonal. The results given in Fig. 4 show that even a sizable change in the shape of the eikonal will not affect much the shape of the differential cross sections there if the elasticity is going to increase.

[11] For the experimental behavior of total and elastic cross sections of hadron-hadron scattering, see Particle Data Group, K. Hikasa *et al.*, Phys. Rev. D **45**, S1 (1992), p. III.83.

[12] E-710 Collaboration, N. A. Amos *et al.*, Phys. Lett. B **247**, 127 (1990).

[13] M. Kawasaki, T. Takaishi, and M. Yonezawa, Phys. Rev. Lett. **67**, 1197 (1991).

[14] A. W. Chao and C. N. Yang, Phys. Rev. D **8**, 2063 (1973).